Physica B 410 (2013) 33–41

Contents lists available at SciVerse ScienceDirect

Physica B

journal homepage: www.elsevier.com/locate/physb

Ternary mixed crystal effects on electron-interface optical phonon interactions in $In_xGa_{1-x}N/GaN$ quantum wells

Wen-Deng Huang [a,b,*], Guang-De Chen [a], Hong-Gang Ye [a], Ya-Jie Ren [b]

[a] MOE Key Laboratory for Nonequilibrium Synthesis and Modulation of Condensed Matter, School of Science, Xi'an Jiaotong University, Xi'an, 710049, China
[b] School of Physics and Telecommunication Engineering, Shaanxi University of Technology, Hanzhong 723001, China

ARTICLE INFO

Article history:
Received 11 August 2012
Received in revised form
29 October 2012
Accepted 6 November 2012
Available online 15 November 2012

Keywords:
Quantum well
Phonon
Electron–phonon interaction

ABSTRACT

Based on the modified random-element isodisplacement model and dielectric continuum model, the dispersions of interface optical phonons, electron-interface phonon interaction and ternary mixed crystal effect on interface optical phonons in $In_xGa_{1-x}N/GaN$ quantum wells are studied in a fully numerical manner. The results indicate that there are two indium concentration intervals that interface optical phonons exist. The indium concentration has important effects on the dispersions and electron–phonon interactions of interface optical phonons. The electron–IO phonon interactions in higher indium concentration are more important than that in lower indium concentration.

1. Introduction

In the last decade, much attention has been focused on group-III nitrides and their alloys due to conspicuous applications in optoelectronic devices, such as the high brightness green/blue InGaN/GaN light-emitting diodes (LEDs) and laser diodes (LDs) [1]. The alloys with different component offer flexible choices for heterostructures and quantum wells (QWs) with matched lattice constants and expected band gaps covered from red to deep ultraviolet [2,3]. The optical phonons and carrier-phonon interactions play an essential role in transport and optical properties of electronic and optoelectronic devices. In order to investigate the optical phonon, many theoretic models have been used. They are microscopic calculation model of the phonon spectra [4], standard dielectric-continuum (DC) model and modified dielectric-continuum (MDC) model [5–7]. The DC model has been extensively employed in the recently literature. Because it describes the properties of optical-phonons in many electronic and optoelectronics devices fabricated from semiconductor nanostructures, including quantum wells, superlattices, quantum wires and quantum dots. Furthermore, experimental data obtained from Raman scattering experiments [8] were found to be in good agreement with the calculations based on the DC model, confirming the correctness of its use for the description of the lattice dynamics properties of wurtzite QWs and superlattices. Therefore, a more thorough description of the phonon modes is unnecessary.

Based on the DC model, many theoretical investigations have been devoted to the polar optical phonons in wurtzite QWs and heterostructures. For example, the polar interface vibrations in AlN/GaN quantum dots were studied in Ref. [9]The frequencies of optical phonon in wurtzite quantum wells (QWs) were studied in Refs. [10,11]. The electron–phonon interactions in QWs composed of binary nitride were investigated in Refs. [12–17]But there still exist substantial problems, most of the experiments have been carried out in III–V QWs composed of ternary alloys [18–21]. To the best our knowledge, the optical phonons and electron–phonon interactions in QWs composed of ternary and quaternary, and even multinary III-nitride wurtzite crystals have not been fully studied. The purpose of the present paper is to study the interface optical (IO) phonons, electron–phonon interactions and ternary mixed crystal effect on interface optical phonons in wurtzite $In_xGa_{1-x}N/GaN$ QWs.

The paper is organized as follows: in Section 2, we present a brief description of model and necessary formula used in calculations. The numerical results for the effect of ternary mixed crystals on the energy of IO phonons and electron–IO phonon interactions in $In_xGa_{1-x}N/GaN$ QWs are given and discussed in Section 3. Finally, the main conclusions are summarized in Section 4.

* Corresponding author at: MOE Key Laboratory for Nonequilibrium Synthesis and Modulation of Condensed Matter, School of Science, Xi'an Jiaotong University, Xi'an, 710049, China. Tel.: +86 091 6264 1630; fax: +86 091 6264 1930.
E-mail address: wdhuang2005@163.com (W.-D. Huang).

0921-4526/$ - see front matter © 2012 Elsevier B.V. All rights reserved.
http://dx.doi.org/10.1016/j.physb.2012.11.004

2. Interface optical phonon modes and electron–phonon interactions in wurtizte quantum wells

2.1. The optical phonons in wurtzite ternary mixed crystals

Group-III nitride and its mixed crystal usually crystallize in the hexagonal wurtzite structure. There are ordinary and extraordinary optical phonons in wurtzite crystals. The extraordinary phonons associated with z- and x–y polarized vibrations, the *z*-polarized mode has $A_1(z)$ symmetry, while the xy-polarized one has $E_1(x,y)$ symmetry. The ordinary phonon is always transverse and polarized in the xy-plane, with $E_1(x,y)$ symmetry [22]. The A_1 and E_1 modes split into longitudinal optical (LO) and transverse-optical (TO) component. Using the modified random-element isodisplacement model [23] and the uniaxial model [24], the frequencies of $A_1(LO)$, $A_1(TO)$, $E_1(LO)$ and $E_1(TO)$ in the wurtzite ternary mixed crystals $A_xB_{1-x}C$ are obtained by the following roots:

$$\omega_{Xi}^2 = \frac{\Omega_{Xbi}^2+\Omega_{Xai}^2}{2} \pm \left[\left(\frac{\Omega_{Xbi}^2-\Omega_{Xai}^2}{2}\right)^2 + x(1-x)\Omega_{Xbai}^4\right]^{1/2}, \tag{1}$$

$$\Omega_{Xbi}^2 = \omega_{bi}^2 + (1-x)\alpha_{Xi}\omega_{bi'}^2, \tag{2}$$

$$\Omega_{Xai}^2 = \omega_{ai}^2 + x_{Xi}\omega_{ai'}^2, \tag{3}$$

$$\Omega_{Xbai}^4 = \left[\left(\frac{\delta_{bi}}{\delta_{ai}}\right)^{1/2}\beta_{Xi}\omega_{bi'}\omega_{ai'} + \frac{\overline{\mu}}{m_C}\omega_{Ai}^2\right] \times \left[\left(\frac{\delta_{ai}}{\delta_{bi}}\right)^{1/2}\beta_{Xi}\omega_{bi'}\omega_{ai'} + \frac{\overline{\mu}}{m_C}\omega_{Bi}^2\right], \tag{4}$$

$$\beta_{Ti} = -\gamma_i, \quad \beta_{Li} = (3-\gamma_i)/\varepsilon_{\infty i}, \tag{5}$$

$$\overline{\mu} = \sqrt{\mu_a\mu_b}, \tag{6}$$

where the subscript *i* stand for *z*- and $\perp$(*x*–*y* plane) polarization directions, *X* stands for longitudinal LO and TO components. μ_a (μ_b) is the reduced mass of wurtzite binary crystal AC (BC), γ_i is introduced parameter which deviates local field from Lorentz relation. We take $\gamma_z = 1-0.1\times(3/4\pi)$ and $\gamma_\perp = 1+0.2\times(3/4\pi)$ [23]. The high-frequency dielectric constant in wurtzite ternary $A_xB_{1-x}C$ can be given out as following:

$$\frac{\varepsilon_{\infty i}-1}{3+\gamma_i(\varepsilon_{\infty i}-1)} = x\frac{v_a}{v}\frac{\varepsilon_{\infty ai}-1}{3+\gamma_i(\varepsilon_{\infty ai}-1)} + (1-x)\frac{\varepsilon_{\infty bi}-1}{3+\gamma_i(\varepsilon_{\infty bi}-1).} \tag{7}$$

The other quantities are given by

$$\omega_{ai}^2 = \omega_{ai}^2\left(1-(1-x)\frac{u_a}{m_C}\right), \tag{8}$$

$$\omega_{ai}'^2 = \left[\delta_{ai}\frac{v_a}{v}\frac{3+\gamma_i(\varepsilon_{\infty i}-1)}{\gamma_i(3+\gamma_i(\varepsilon_{\infty ai}-1)}(\omega_{Ai}^2-\omega_{Tai}^2)\right], \tag{9}$$

$$\omega_{Ai}^2 = \frac{3+(\varepsilon_{\infty ai}-1)}{3+\gamma_i(\varepsilon_{\infty ai}-1)}\omega_{Tai}^2, \tag{10}$$

$$\delta_{ai} = 1-x\frac{u_a}{m_C}\left(1-\frac{e_{bi}}{e_{ai}}\right). \tag{11}$$

by interchanging *a* by *b* and *x* by $1-x$, we can obtained the other variables ω_{bi}, ω_{bi}, ω_{Ai} and δ_{bi}.

2.2. The interface optical phonons and electron-interface phonon interactions in wurtizte quantum wells.

We consider an arbitrary wurtzite symmetry multilayer heterostructures. The interfaces are located at $z=z_j(j=0,1,\ldots,n-1)$. We take the *z* axis along the direction of the *c* axis. There exist five distinct types of optical-phonon modes in the wurtzite multilayer heterostructures. They are IO phonon modes, propagating optical phonon modes, quasi-confined optical phonon modes, half-space optical phonon modes, and exactly confined modes [15,17]. In this paper, we will solve the IO phonon modes and electron–phonon interactions by using the determinate method. The two dimensional *p*-polarization fields $\pi(q_\perp, z)$ of the IO phonons in the layer *j* can be obtained from the *p*-polarization field motion Eqs. [11–13]:

$$\pi_\perp^{(j)}(P_\perp,P_z) = \begin{cases} B_0 e^{q_{z,0}(z-z_0)}[i,\gamma_0], z<z_0, \\ [\left(A_j' e^{-q_{z,j}(z-z_j)} + B_j' e^{q_{z,j}(z-z_j)}\right), \gamma_j\left(-A_j' e^{-q_{z,j}(z-z_j)} + B_j' e^{q_{z,j}(z-z_j)}\right)], \quad z_{j-1}<z<z_j, \\ A_n' e^{-q_{z,n}(z-z_{n-1})}[1,\gamma_n], \quad z_{n-1}<z<\infty. \end{cases} \tag{12}$$

Here $\gamma_j (j=0,1,2,\ldots n)$ is given in Ref. [13]. Using the boundary conditions based on DC model [12,14] at the $z=z_j$ interface successively, the dispersion relation of IO phonons can be obtained by the below $2n\times 2n$ determinant.

$$\begin{vmatrix}
a_0 & b_1 & b_1' & 0 & 0 & 0 & 0 & 0 & 0 & 0 & 0 & 0 & 0 & 0 & 0 & 0 \\
a_0' & c_1 & c_1' & 0 & 0 & 0 & 0 & 0 & 0 & 0 & 0 & 0 & 0 & 0 & 0 & 0 \\
0 & a_1 & a_1 & b_2 & b_2' & \ldots & 0 & 0 & 0 & 0 & 0 & 0 & 0 & 0 & 0 & 0 \\
0 & a_1' & -a_1' & c_2 & c_2' & \ldots & 0 & 0 & 0 & 0 & 0 & 0 & 0 & 0 & 0 & 0 \\
0 & 0 & 0 & a_2 & a_2 & \ldots & 0 & 0 & 0 & 0 & 0 & 0 & 0 & 0 & 0 & 0 \\
0 & 0 & 0 & a_2' & -a_2' & \ldots & 0 & 0 & 0 & 0 & 0 & 0 & 0 & 0 & 0 & 0 \\
0 & 0 & 0 & 0 & 0 & \ldots & a_j & a_j & b_{j+1} & b_{j+1}' & 0 & 0 & 0 & 0 & 0 & 0 \\
0 & 0 & 0 & 0 & 0 & \ldots & a_j' & -a_j' & c_{j+1} & c_{j+1}' & 0 & 0 & 0 & 0 & 0 & 0 \\
0 & 0 & 0 & 0 & 0 & \ldots & 0 & 0 & 0 & 0 & 0 & 0 & 0 & a_{n-1} & a_{n-1} & -a_n \\
0 & 0 & 0 & 0 & 0 & \ldots & 0 & 0 & 0 & 0 & 0 & 0 & 0 & a_{n-1}' & -a_{n-1}' & -a_n'
\end{vmatrix} \tag{13}$$

In Eq. (13), we define

$$\begin{aligned}
&a_j = \chi_{\perp j}^{-1}, && a_j' = -\tfrac{\varepsilon_{z,j} q_{z,j}}{\chi_{\perp j} q_\perp}, \\
&b_j = -\chi_{\perp j}^{-1} e^{-q_{z,j}(z_j - z_{j+1})}, && b_j' = -\chi_{\perp j}^{-1} e^{q_{z,j}(z_j - z_{j+1})}, \\
&c_j = \tfrac{\varepsilon_{z,j} q_{z,j}}{\chi_{\perp j} q_\perp} e^{-q_{z,j}(z_j - z_{j+1})}, && c_j' = -\tfrac{\varepsilon_{z,j} q_{z,j}}{\chi_{\perp j} q_\perp} e^{q_{z,j}(z_j - z_{j+1})}.
\end{aligned} \tag{14}$$

From the Eq. (13), we can obtain the dispersion relation of single wurtizte symmetry quantum wells as following:

$$2q_{z,0}\varepsilon_{z,0} q_{z,1}\varepsilon_{z,1} + \frac{q_{z,0}^2\varepsilon_{z,0}^2 + q_{z,1}^2\varepsilon_{z,1}^2}{q_{z,0}\varepsilon_{z,0} q_{z,1}\varepsilon_{z,1}} \tanh(q_{z,1} d_1) = 0. \tag{15}$$

In Eq. (15), we use index 1 for quantum well material and 0 for the barrier material, d_1 is the width of the quantum well. Generally, Eq. (15) has a definite number solutions with definite symmetry with respect to symmetric center of the QW structure for a given phonon wave vector $q_\perp$ (see Figs. 3 and 4). Our numerical calculations show that the IO phonons exist in different frequency range with different concentration of indium (x) in $In_xGa_{1-x}N$/GaN QWs.

By using a standard quantization procedure [25–27], the electron–phonon interaction Hamiltonian for the IO phonon modes in wurtzite multilayer heterostructures can be obtained as follows:

$$H_{e-ph} = \sum_m \sum_{q_\perp} e^{i\vec{q}_\perp \cdot \vec{\rho}}\, \Gamma_m(q_\perp, z)[\hat{\alpha}_m(\vec{q}_\perp) + \hat{\alpha}_m^+(-\vec{q}_\perp)]. \tag{16}$$

where $\Gamma_m(q_\perp, z)$ is electron–phonon coupling functions, which describe the coupling strength of single electron at the position z with the mth IO phonon modes, and is given by

$$\Gamma_m(q_\perp, z) = B_0\left(\frac{\hbar e^2}{8A\varepsilon_0\omega_m(q_\perp)}\right)^{1/2} \begin{cases} f_1(q_\perp, z), & z < z_0, \\ f_2(q_\perp, z), & z_{j-1} < z < z_j, \quad j = 1,2,3\cdots\cdots n-1. \\ f_3(q_\perp, z), & z > z_n, \end{cases} \tag{17}$$

where A is the cross-sectional area of the heterostructures, the normal frequency $\omega_m(q_\perp, z)$ of the mth branch of the IO phonon modes can be obtained by solving the dispersion relation Eq. (10), and $f_i\ (q_\perp, z)\ (i=1, 2, 3)$ are defined as

$$\begin{aligned}
f_1(q_\perp, z) = {} & \alpha_{-,0} e^{q_\perp(z-z_0)} + (\alpha_{+,0} - \alpha_{-,0}) e^{q_{z,0}(z-z_0)} + D_{2n-1} a_{+,n} e^{q_\perp(z-z_{n-1})} \\
& + \sum_{j=1}^{n-1} [\left(D_{2j} a_{-,j} - D_{2j-1} a_{+,j}\right) e^{q_\perp(z-z_l)} - \left(D_{2j-1} a_{+,j} e^{q_{z,j} d_j} - D_{2j} a_{-,j} e^{-q_{z,j} d_j}\right) e^{q_\perp(z-z_{j-1})}],
\end{aligned} \tag{18}$$

$$\begin{aligned}
f_2(q_\perp, z) = {} & \alpha_{+,0} e^{q_\perp(z-z_0)} + \sum_{l=1}^{j-1} [(D_{2l} a_{+,l} - D_{2l-1} a_{-,l}) e^{q_\perp d_l} + \left(D_{2l-1} a_{-,l} e^{q_{z,l} d_l} - D_{2l}^* a_{+,l} e^{-q_{z,l} d_l}\right)] e^{-q_\perp(z-z_{l-1})} \\
& + \left(D_{2j-1} e^{-q_{z,j}(z-z_j)} + D_{2j-1} e^{q_{z,j}(z-z_j)}\right)(a_{+,j} - a_{-,j}) + \left(D_{2j-1} a_{-,j} e^{q_{z,l} d_j} - D_{2j} a_{+,j} e^{-q_{z,j} d_j}\right) e^{-q_\perp(z-z_{j-1})} \\
& + \sum_{l=j+1}^{n-1} [(D_{2l} a_{-,l} - D_{2l-1} a_{+,l}) e^{-q_\perp d_l} + D_{2l-1} a_{+,j} e^{q_{z,l} d_l} - D_{2j} a_{-,j} e^{-q_{z,j} d_j}] e^{q_\perp(z-z_{l-1})} + D_{2n-1} a_{+,n} e^{q_\perp(z-z_{n-1})}
\end{aligned} \tag{19}$$

$$\begin{aligned}
f_3(q_\perp, z) = {} & \alpha_{+,0} e^{q_\perp(z-z_0)} + \sum_{l=1}^{n-1} [(D_{2l} a_{+,l} - D_{2l-1} a_{-,l}) e^{q_\perp d_l} + D_{2l-1} a_{-,j} e^{q_{z,l} d_l} - D_{2j} a_{+,j} e^{-q_{z,j} d_j}] e^{q_\perp(z-z_{l-1})} \\
& + D_{2n-1} [e^{-q_{z,n}(z-z_{n-1})}(a_{+,n} - a_{-,n}) - a_{-,n} e^{-q_\perp(z-z_{n-1})}].
\end{aligned} \tag{20}$$

In Eqs. (17–19)

$$a_{\pm j} = \frac{1 \pm \gamma_j}{q_{z,j} \pm q_\perp} \tag{21}$$

D_0, D_j can be obtained by the determinant method as following:

$$D_0 = \begin{vmatrix} b_1 & b_1' & 0 & 0 & 0 & 0 & 0 & 0 & 0 & 0 & 0 & 0 & 0 & 0 & 0 \\ c_1 & c_1' & 0 & 0 & 0 & 0 & 0 & 0 & 0 & 0 & 0 & 0 & 0 & 0 & 0 \\ a_1 & a_1 & b_2 & b_2' & \cdots & 0 & 0 & 0 & 0 & 0 & 0 & 0 & 0 & 0 & 0 \\ a_1' & -a_1' & c_2 & c_2' & \cdots & 0 & 0 & 0 & 0 & 0 & 0 & 0 & 0 & 0 & 0 \\ 0 & 0 & 0 & a_2 & a_2 & \cdots & 0 & 0 & 0 & 0 & 0 & 0 & 0 & 0 & 0 \\ 0 & 0 & 0 & a_2' & -a_2' & \cdots & 0 & 0 & 0 & 0 & 0 & 0 & 0 & 0 & 0 \\ 0 & 0 & 0 & 0 & 0 & \cdots & a_j & a_j & b_{j+1} & b_{j+1}' & \cdots & 0 & 0 & 0 & 0 \\ 0 & 0 & 0 & 0 & 0 & \cdots & a_j' & -a_j' & c_{j+1} & c_{j+1}' & \cdots & 0 & 0 & 0 & 0 \\ 0 & 0 & 0 & 0 & 0 & 0 & 0 & 0 & 0 & 0 & 0 & 0 & a_{n-1} & a_{n-1} & -a_n \end{vmatrix} \quad (22)$$

Table 1
Optical phonon energies (in meV), dielectric constants, effective charge (in e_0) and other parameters in calculations.

Material	$\omega_{z,T}$	$\omega_{\perp,T}$	$\omega_{z,L}$	$\omega_{\perp,L}$	$\varepsilon_{\infty,z}$	$\varepsilon_{\perp,z}$	e_z	$e_\perp$	a	c
GaN	65.91[a]	69.25[a]	90.97[a]	91.83[a]	6.38[b]	6.11[b]	2.86[b]	2.69[b]	3.20[b]	5.22[b]
InN	55.27[c]	58.87[c]	70.14[c]	73.45[b]	7.96[b]	7.61[b]	2.96[b]	2.78[b]	3.48[b]	5.64[b]

[a] Reference [29].
[b] Reference [30].
[c] Reference [28].

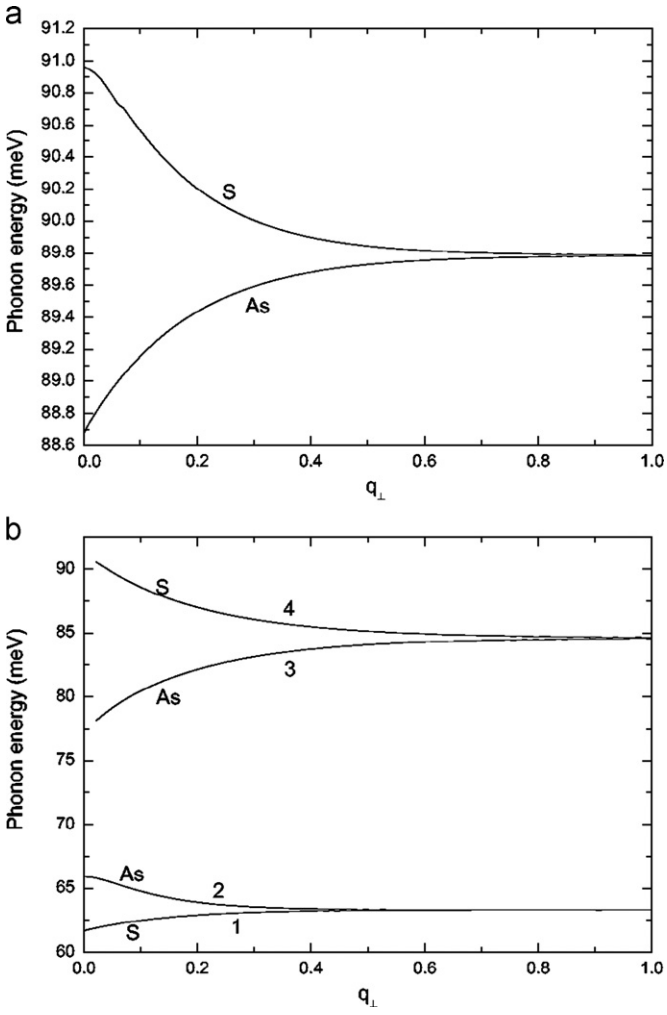

Fig. 1. Dispersion curves of IO phonon modes for an $In_xGa_{1-x}N$ QW of width $d=5$ nm sandwiched between two semi-infinite GaN barrier layers. Here (a) for $x=0.2$, and (b) for $x=0.8$.

$$D_j = \begin{bmatrix} b_1 & b_1' & 0 & 0 & 0 & \dots & a_0 & \dots & 0 & 0 & 0 & 0 & 0 & 0 & 0 & 0 & 0 \\ c_1 & c_1' & 0 & 0 & 0 & \dots & a_1' & \dots & 0 & 0 & 0 & 0 & 0 & 0 & 0 & 0 & 0 \\ a_1 & a_1 & b_2 & b_2' & \dots & \dots & 0 & \dots & 0 & 0 & 0 & 0 & 0 & 0 & 0 & 0 & 0 \\ a_1' & -a_1' & c_2 & c_2' & \dots & \dots & 0 & \dots & 0 & 0 & 0 & 0 & 0 & 0 & 0 & 0 & 0 \\ 0 & 0 & 0 & a_2 & a_2 & \dots & 0 & \dots & 0 & 0 & 0 & 0 & 0 & 0 & 0 & 0 & 0 \\ 0 & 0 & 0 & a_2' & -a_2' & \dots & 0 & \dots & 0 & 0 & 0 & 0 & 0 & 0 & 0 & 0 & 0 \\ 0 & 0 & 0 & 0 & 0 & \dots & 0 & \dots & a_j & a_j & b_{j+1} & b_{j+1}' & 0 & 0 & 0 & 0 & 0 \\ 0 & 0 & 0 & 0 & 0 & \dots & 0 & \dots & a_j' & a_j' & c_{j+1} & c_{j+1}' & 0 & 0 & 0 & 0 & 0 \\ 0 & 0 & 0 & 0 & 0 & \dots & 0 & \dots & 0 & 0 & 0 & 0 & 0 & 0 & a_{n-1} & a_{n-1} & -a_n \end{bmatrix} \quad (23)$$

D_0, and D_j are $2n \times 2n$ determinants, the jth column in D_j was substituted by the column matrix (α_0, α_0', 0, 0…0, 0).

3. Numerical results and discussion

In order to further understand ternary mixed crystals effects on IO phonons and electron–phonon interactions in wurtizte In_xGa_{1-x}/GaN QWs more clearly. Numerical calculations on $In_xGa_{1-x}N$/GaN single QW have been performed. The corresponding physical parameters [28–30] are listed in Table 1. In our calculation, we do not consider the strain effects of QW, because the behavior of IO phonons in strained QWs is similar to those in unstrained QWs [13].

The dispersions of IO phonons in GaN/In_xGa_{1-x}N/GaN symmetry single QW are plotted in Fig. 1. We can see that the IO phonons exist in high frequency range ($\omega_{\perp,\,L1}$, $\omega_{\perp,\,L0}$) or low frequency range ($\omega_{\perp,\,T1}$, $\omega_{\perp,\,T0}$). The indium concentration (x) has many effects on the branches and frequency ranges of the IO phonons. If the indium concentration x is in the interval (0.05, 0.40), there are two IO phonon branches in high frequency range, and no IO phonon branches in low frequency range. When the indium concentration x is in the interval (0.40, 1.00), there exist four IO phonon branches in two frequency ranges. When the indium concentration x is in the range (0.00, 0.05),

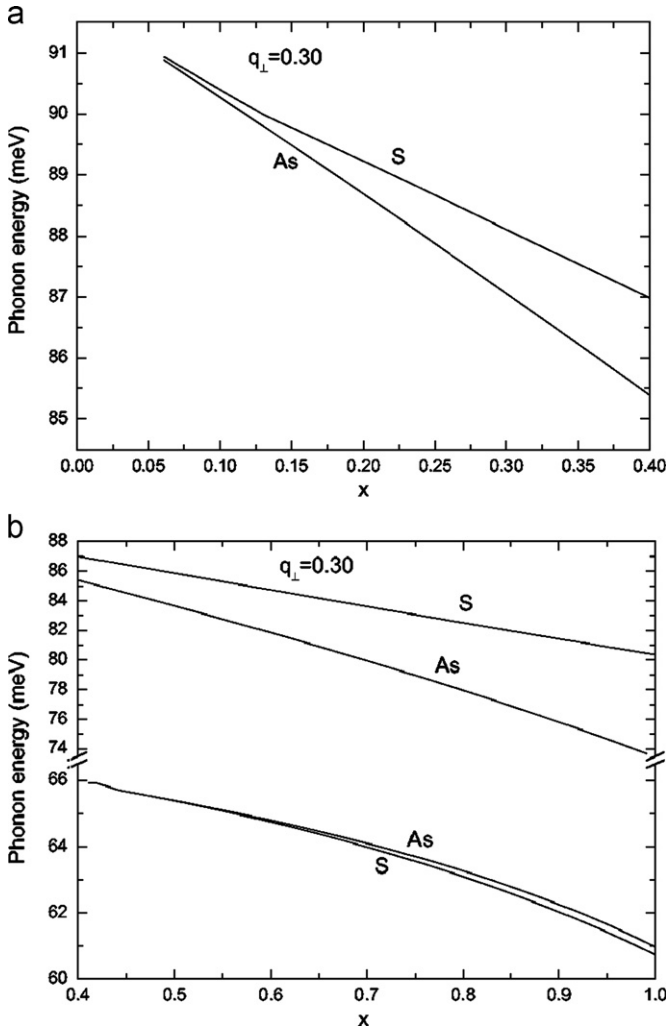

Fig. 2. The effects of indium concentration (x) on dispersion curves of IO phonons for the same QW as in Fig. 1 ($q_\perp = 0.30$). Here (a) for $0.05 < x < 0.4$, and (b) for $0.4 < x < 1.0$.

there no IO phonons. In the Refs. [14–17], the IO phonons exist in high frequency range ($\omega_{\perp,\,L1}$, $\omega_{\perp,\,L0}$) and low frequency range ($\omega_{\perp,\,T1}$, $\omega_{\perp,\,T0}$), the branches of IO phonons is four, which is different from our numerical results. In Ref. [16], the authors have also considered existence of interfacial transition regions, the frequencies of IO change with increase of the width of QW. If we consider this, we can obtain the similar results. From the Fig. 1, we can observe that the frequencies of interface optical phonons in low frequency range approach a common limit in the case of $q_\perp \to \infty$. For the high frequency range, another common limit can be reached. Furthermore, the common limit in each frequency range is different with different indium concentration x. The effects of mixed crystal affect the behavior of IO phonons in QWs greatly.

The IO phonon frequencies as function of indium concentration (x) are plotted in Fig. 2. We can see that the frequencies of IO phonons in high frequency range decrease almost linearly with increasing indium concentration if x is in the interval (0.05, 0.40). When the indium concentration x is in the interval (0.40, 1.00), the frequencies of IO phonons in high frequency range still decrease with increasing indium concentration, but for the IO phonons in low frequency range, it do not vary almost linearly with concentration changes. So the empirical formula in Ref. [28] cannot been used to investigate all kinds of phonon modes in quantum wells composed of wurtzite mixed crystal. The mixed crystal effects change greatly the phonon modes in the QWs, and appear in many optical and electronic experiments which related to the phonon modes and phonon frequencies. In recent years, extensive investigations have been carried out by Raman scattering experiment, the IO phonon modes were observed [18–21]. We believe that our numerical calculation will be helpful to the experiment.

Figs. 3 and 4 show the electron–IO phonon coupling functions $\Gamma_m(q_\perp, z)$ which describes the strength of electron–phonon interaction. Our calculations clearly indicate that electron–IO phonon coupling function has exactly symmetry with respect to the center of the quantum wells at $z=2.5$ nm. If the indium concentration x is in the interval (0.05, 0.40) (please see the Fig. 3), the electron–IO phonon coupling function for the symmetric modes are greater than that for the anti-symmetric modes. We can see from these figures that the electron–IO phonon interactions are mainly located at quantum wells. When z goes to infinity, the electron–IO phonon interactions decrease to 0. From our calculations, we can also see that the long-wavelength optical phonons are more important than short wavelength optical phonons for electron–phonon interaction. The electron–IO phonon coupling function for symmetric modes are more important than anti-symmetric modes. If indium concentration x is in the interval (0.40, 1.00), (please see the Fig. 4), the modes 1 and 4 (2 and 3) (labeled from lower to higher frequency) are exactly symmetric (anti-symmetric) modes with respect to the center of the QW

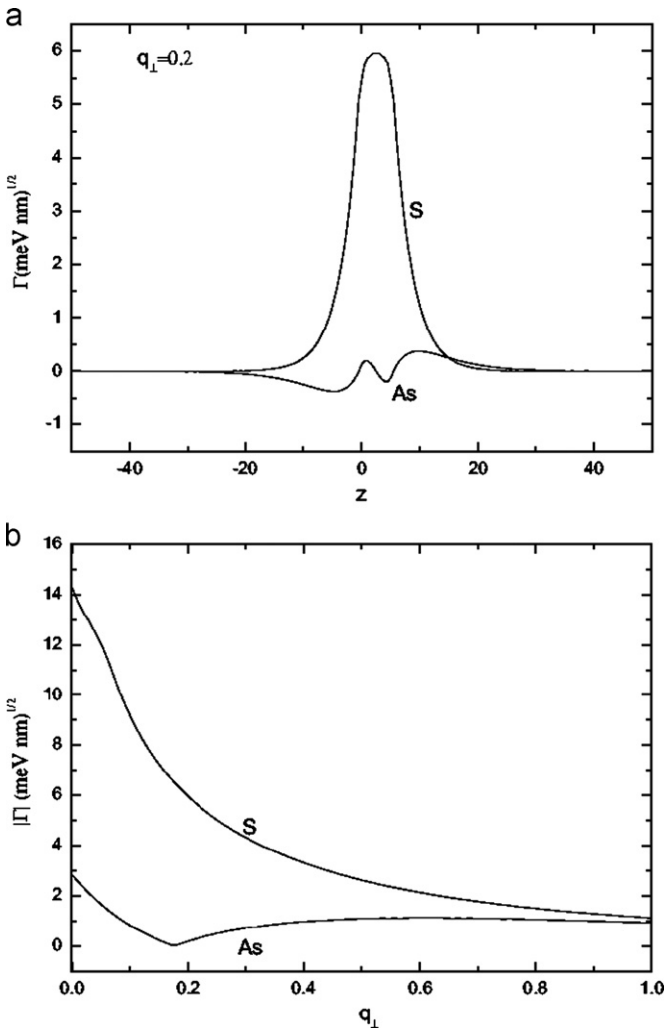

Fig. 3. Electron–IO phonon coupling functions $\Gamma_m(q_\perp, z)$ in the same QW as in Fig. 1 with indium concentration $x=0.2$: (a) the spatial dependence of the electron–IO phonon coupling functions $\Gamma_m(q_\perp, z)$ with the wave number $q_\perp=0.20$ and (b) the wave-vector dependence of the electron–IO phonon coupling functions $\Gamma_m(q_\perp, z)$ with $z=5$nm.

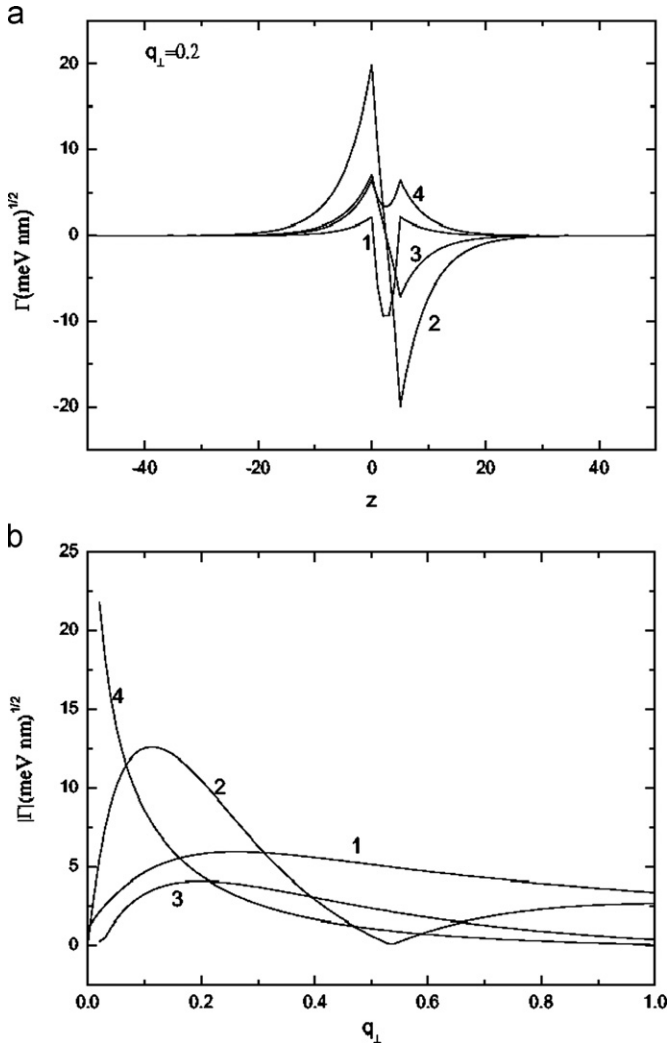

Fig. 4. Same as in Fig. 3, but for $x=0.8$.

structure. The modes 2 and 4 have more important effects on electron–phonon interactions when the wave number $q_\perp$ is smaller than 0.18. When $q_\perp$ is greater than 0.18, the modes 1 have most important effects on electron–phonon interactions. Comparing Fig. 3 with Fig. 4, we can draw a conclusion that the electron–IO phonon interactions with higher indium concentration (x) are more important. Our numerical results indicate that the behavior of electron–IO phonon in $In_xGa_{1-x}N$/GaN QWs is very different from that in QWs composed of binary crystal [11–13].The ternary mixed crystal effects influence the electron–IO phonon interactions, which also observed by Raman Spectroscopy experiments [20].

In order to see the effects of ternary mixed crystals on electron–IO phonon interactions, the electron–IO phonon coupling function $\Gamma_m(q_\perp, z)$ as function of indium concentration (x) are plotted in Fig. 5. If x is in the interval (0.05, 0.40), we can observe that the electron–phonon interaction for symmetric mode increase, and reach a maximum (at $x=0.09$), then decrease linearly with the increasing indium concentration. For the anti-symmetric modes, their electron–phonon interaction decrease linearly. If x is in the interval (0.40, 1.00), we can see that the electron–phonon interaction of IO phonons (modes 1 and 2) in low frequency range decrease linearly with the increase of indium concentration. For the IO phonons in high frequency range, their electron–phonon interactions indicate non-linear changes with increasing indium concentration (x). The symmetric modes are non-linear increase, and the anti-symmetric modes are non-linear decrease.

4. Conclusion

Within the framework of the modified random-element isodisplacement model and DC model, we have studied the IO phonons and electron–phonon interaction in wurtizte $In_xGa_{1-x}N$/GaN QWs. The ternary mixed crystal effects influence the IO phonon and electron–IO phonon interactions. When the indium concentration (x) is in the range (0.05, 0.40), only two branches appear in high frequency range. When x is in the range (0.40, 1.00), the IO phonons appear in high frequency range and low frequency range, the branches of four. The electron–IO phonon interactions in higher indium concentration (x) are more important.

These results and conclusion are important and useful for further theoretical investigations of phonon effect in arbitrary wurtzite Q2D multilayer heterostructures, can be directly applied to many important multilayer heterostructures, such as quantum wells, superlattices, quantum wires and quantum dots composed of Group III ternary and quaternary, and even multinary group III-nitride wurtzite

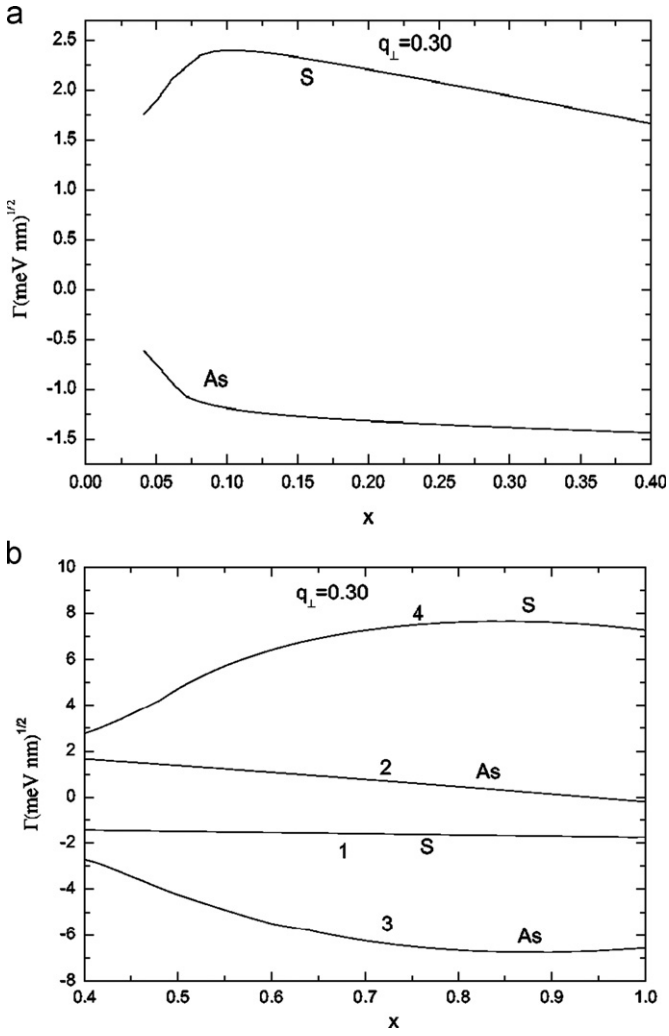

Fig. 5. The effect of indium concentration (x) on electron–phonon coupling functions $\Gamma_m(q_\perp, z)$ for the IO phonons in the same QW as in Fig. 1 ($q_\perp$=0.30). Here (a) for $0.05 < x < 0.40$, and (b) for $0.40 < x < 1.00$.

crystals. Our results are also important and helpful for further investigation of phonons in experimental techniques, such as the inelastic light scattering spectroscopy of Raman and Brillouin types.

Acknowledgment

This work was supported by the National Natural Science Foundation of China (Grant nos. 11074200 and 51106093), Scientific Research Program Funded by Shaanxi Provincial Education Department (Grant no. 12JK0982) and Natural Science Basic Research Plan in Shaanxi Province of China (Grant no. 2011JM1016).

References

[1] S. Nakamura, G. Fasol, The Blue Laser Diodes: GaN Light Emitters and Lasers, Springer, Berlin, 1997.
[2] J. Li, K.B. Nam, K.H. Kim, J.Y. Lin, H.X. Jiang, Appl. Phys. Lett. 78 (2001) 61.
[3] H. Hirayama, A. Kinoshita, T. Yamabi, Y. Enomoto, A. Hirata, T. Araki, Y. Nanishi, Y. Aoyagi, Appl. Phys. Lett. 80 (2002) 207.
[4] K.P. Bohnen, R. Heidl, M. Krauss, Europhys. Lett. 64 (2003) 104.
[5] E.L. Albuquerque, J. Phys. C 13 (1980) 2623.
[6] M. Babiker, D.R. Tilley, E.L. Albuquerque, C.E.T. Goncalves da Silva, J. Phys. C: Solid State Phys. 18 (1985) 1269.
[7] M. Babiker, D.R. Tilley, E.L. Albuquerque, J. Phys. C: Solid State Phys. 18 (1985) 1285.
[8] H. Rücker, E. Molinari, P. Lugli, Phys. Rev. B 45 (1992) 6747.
[9] D. Romanov, V. Mitin, M. Stroscio, Phys. Rev. B 66 (2002) 115321.
[10] S.M. Komirenko, K.W. Kim, M.A. Stroscio, Phys. Rev. B 59 (1999) 5013.
[11] B.C. Lee, K.W. Kim, M.A. Stroscio, M. Dutta, Phys. Rev. B 58 (1998) 4860.
[12] J. Gleize, M.A. Renucci, J. Frandon, F. Demangeot, Phys. Rev. B 60 (1999) 15985.
[13] J.J. Shi, Phys. Rev. B 68 (2003) 165335.
[14] J.J. Shi, X.L. Chu, Phys. Rev. B 70 (2004) 115318.
[15] J.T. Lü, J.C. Cao, Phys. Rev. B 71 (2005) 155304.
[16] E.L. Albuquerque, R.C. Vilela, E.F. Nobre, R.N. Costa Filho, V.N. Freire, G.A. Farias, Solid State Commun. 135 (2005) 308.
[17] Z.W. Zuo, H.J. Xie, Phys. Lett. A 37 (2011) 2007.

[18] J. Ibáñez, A. Rapaport, C. Boney, et al., J. Raman Spectrosc. 43 (2012) 237.
[19] Hiroshi Harima, J. Phys.: Condens. Matter 14 (2002) R967.
[20] C. Faugeras, G. Martinez1, F. Capotondi, G. biasiol, L. Sorba, Europhys. Lett. 67 (2004) 1031.
[21] M. Dutta, D. Alexson, L. Bergman, Physica E 11 (2001) 277.
[22] R. Loudon, Adv. Phys. 13 (1964) 423.
[23] S.G. Yu, K.W. Kim, Leah Bergman, Phys. Rev. B 58 (1998) 15283.
[24] W. Hayes, R. Loudon, Scattering of Light by Crystal, Wiley, New York, 1978.
[25] H. Haken, Quantum Field Theory of Solids, North-Holland, Amsterdam, 1976.
[26] L. Wendler, Phys. Status Solidi B 129 (1985) 513.
[27] L. Wendler, R. Haupt, Phys. Status Solidi B 143 (1987) 487.
[28] D. Behr, R. Niebuhr, J. Wagner, K.H. Bachem, U. Kaufmann, In Galliun and Related Materials II, in: C.R. Abernathy, H. Amano, J.C. Zolper (Eds.), Materials Research Society, Pittsburgh, 1997.
[29] A. Kasic, M. Schubert, J. Off., et al., Phys. Status Solidi C 0 (2003) 1750.
[30] C. Burgaro, K. Rapcewicz, J. Bernholc, Phys. Rev. B 61 (2000) 6720.